

SNeCT: Scalable network constrained Tucker decomposition for integrative multi-platform data analysis

Dongjin Choi

Seoul National University
skywalker5@snu.ac.kr

Lee Sael

The State University of New York (SUNY) Korea
sael@sunykorea.ac.kr

ABSTRACT

Motivation: How do we integratively analyze large-scale multi-platform genomic data that are high dimensional and sparse? Furthermore, how can we incorporate prior knowledge, such as the association between genes, in the analysis systematically?

Method: To solve this problem, we propose a Scalable Network Constrained Tucker decomposition method we call SNeCT. SNeCT adopts parallel stochastic gradient descent approach on the proposed parallelizable network constrained optimization function. SNeCT decomposition is applied to tensor constructed from large scale multi-platform multi-cohort cancer data, PanCan12, constrained on a network built from PathwayCommons database.

Results: The decomposed factor matrices are applied to stratify cancers, to search for top- k similar patients, and to illustrate how the matrices can be used for personalized interpretation. In the stratification test, combined twelve-cohort data is clustered to form thirteen subclasses. The thirteen subclasses have a high correlation to tissue of origin in addition to other interesting observations, such as clear separation of OV cancers to two groups, and high clinical correlation within subclusters formed in cohorts BRCA and UCEC. In the top- k search, a new patient's genomic profile is generated and searched against existing patients based on the factor matrices. The similarity of the top- k patient to the query is high for 23 clinical features, including estrogen/progesterone receptor statuses of BRCA patients with average precision value ranges from 0.72 to 0.86 and from 0.68 to 0.86, respectively. We also provide an illustration of how the factor matrices can be used for interpretable personalized analysis of each patient.

Availability: The code and data available at our repository¹.

Supplementary information: Supplementary data are available at *Bioinformatics* online.

1 INTRODUCTION

Integrative analysis of multiple perspectives of a patient helps in both stratification and clinical predictions. Stratification helps the researchers in understanding and exploring the genomic characteristics in relation to their current phenotypes and thus to recognize opportunities for clinical improvement on stratified groups of patients. In the perspective of personalized medicine, clinical diagnostics and predictions of individual patient is needed and can be done by searching the integrated profile of a patient to existing records. Analysis of one or few data types may not be sufficient for stratifications or accurate predictions of disease as they only provide partial information about the patient's biological status.

Related works in integrative genomic analysis: Need for integrative data analysis methods is being recognized, however, due

to increased size of data and a limited number of uniform data analysis framework, integrative analysis of multiple data types is still a challenging task. Existing methods are often limited in interpretability and scalability and often runs in selected subset of data and features. Other methods run only on small number of genes such as work by [14] that shows the effect of DNA methylation and CNV in gene expression of several known oncogenes for glioblastoma and ovarian cancer; PARADIGM method by [29] that adopts graph inference approach on augmented pathway structure containing nodes for CNV, gene expression, protein expression and active protein information; and a work by [24] that proposes an integrative statistical framework based on a sparse regression of gene expression values based on CNV, miRNA, and methylation. Many methods run only on small data sets, such as multiple-kernel based method by [26, 27] that combines kernels generated from individual platform data in a weighted linear fashion for stratification and predictions of ovarian cancer; a method by [15] that applies multivariate Cox Lasso model and median time-to-event prediction algorithm on dataset integrated from the CNV, methylation, miRNA, and gene expression data; and iCluster method by [17] that transforms multi-platform data to latent space and clusters using latent variable. Also, many methods do not truly integrate the data in the analysis such as work by [30] that evaluated the predictive power of patient survival and clinical outcome using clinical data in combination with one of CNV, methylation, mRNA, miRNA or protein expression data, and work by [5] that stratifies the PANCAN12 dataset using multi-platform data where clustering results of each data type are used to construct the final cluster. **Multi-platform multi-cancer data analysis:** The data scalability challenge in the integrative analysis is even more evident in multi-platform data analysis across multiple cancer types. Analysis across multiple cancer types enables us to get a glimpse of the extent to which genomic signatures are shared across the different cancers. The biological understanding of similarity and dissimilarity among the different cancer types can enable efficient management of diseases as well as treatment transfers between different cancer types of similar genomic signatures. The work of [5] is one of the first attempts to utilize multi-platform data of multiple cancers, i.e. the PanCan12 dataset. The PanCan12 dataset is created by the Pan-Cancer initiative that compares 12 tumor types profiled by The Cancer Genome Atlas (TCGA) Research Network and includes data from six different platforms [3]. In their work, integrated subtype classification for all of the tumor samples was performed by first clustering on individual data platforms, and then using the results of single-platform clusters as input to a second-level cluster analysis to form a cluster-of-cluster assignment (COCA). Fully integrative data analysis method would consider and optimize the multi-platform data altogether. In this perspective, the

¹ <https://github.com/skywalker5/SNeCT>

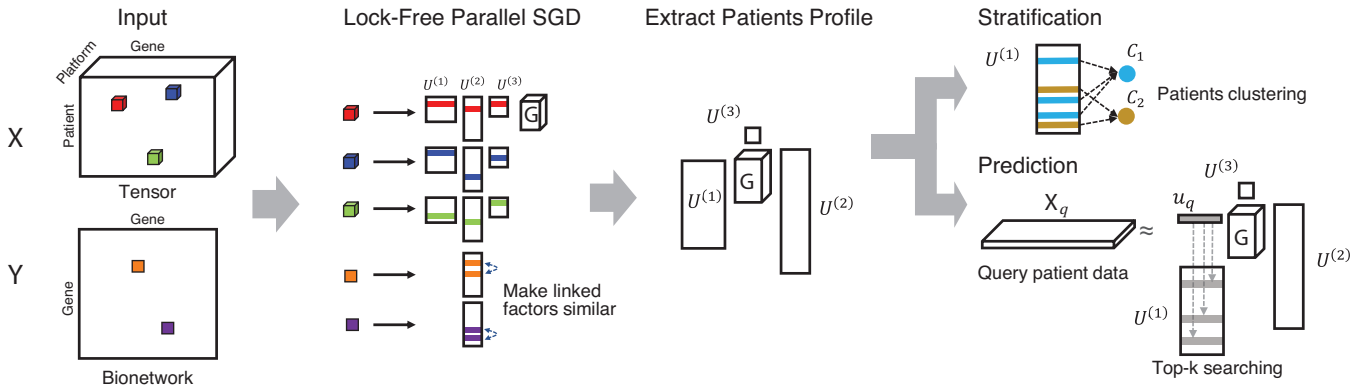


Figure 1: Overview of the tensor decomposition of SNeCT and validation processes.

COCA method can be considered as an ensemble method where the input data are varied, rather than an integrative method. Also, it is difficult to utilize the COCA approach for finding similar patients as needed in the clinical predictions given a new patient’s data without redoing the analysis over again. Thus, there is a need for multi-platform data analysis method that can scalably stratify multiple cancer types for knowledge discovery and predict clinical outcomes for enabling personalized medicine.

Related works in tensor analysis: Tensors, i.e., multi-dimensional arrays, are a natural representation of multi-platform genomic data [22]. The core of tensor analysis is tensor decomposition, which can be considered as higher-order singular value decomposition (HOSVD). Tensor analysis has been widely applied with success on network traffic [16], knowledge bases [1, 19], hyperlinks and anchor texts in the Web graphs [10], sensor streams [25], and DBLP conference-author-keyword relations [12], to name a few. The major challenge of tensor analysis is data scalability as there is an intermediate data explosion problem in the decomposition process even when the input tensor fits into the memory. To address this problem we have previously proposed a Hadoop based parallel tensor decomposition method [6, 7] and a multi-core based method [23].

Contributions: In this paper, we propose a tensor-based method that enables stratification and clinical prediction of patients utilizing multi-platform data analysis across multiple cancer types. We have shown in our previous works [8, 9] that somatic mutation profiles generated from orthogonal matrix decomposition enable accurate stratification and clinical predictions of each cancer type. We extend this approach to multi-platform multi-cancer data analysis by proposing a scalable network constrained Tucker decomposition (SNeCT) method (Figure 1), and show that SNeCT can efficiently stratify cancer subtypes and predict clinical outcomes. The contributions of this paper are listed in the following.

- A novel scalable network constrained Tucker decomposition (SNeCT) algorithm.
- Stratification on multi-platform multi-cohort data showing similarity and difference between cancer cohorts.

- Individualized clinical prediction utilizing multi-platform genomic profiles.
- A demonstration of personalized interpretation utilizing factor matrices.

2 MATERIALS AND METHODS

2.1 Data processing

2.1.1 Tensor construction with the PanCan12. Initially, Pan-Cancer-12 data freeze version 4.7 was downloaded from the Sage Bionetworks repository, Synapse [20]. The PanCan12 contains multi-platform data with mapped clinical information of patients group into cohorts of twelve cancer type: bladder urothelial carcinoma (BLCA), breast adenocarcinoma (BRCA), colon and rectal carcinoma (COAD, READ), glioblastoma multiforme (GBM), head and neck squamous cell carcinoma (HNSC), kidney renal clear cell carcinoma (KIRC), acute myeloid leukaemia (LAML), lung adenocarcinoma (LUAD), lung squamous cell carcinoma (LUSC), ovarian serous carcinoma (OV), and uterine corpus endometrial carcinoma (UCEC). Table 1 lists the Synapse IDs of the downloaded data for each platform used. After download, probes of each platform are mapped to corresponding gene symbols. Then, subjects and genes that have less than two evidences are removed from the dataset. The resulting data for each platform are min-max normalized and is further normalized such that the Frobenius norm, i.e., $\|A\| \equiv \sqrt{\sum_i \sum_j |a_{ij}|^2}$, becomes one. A cell of resulting 3-mode tensor, \mathcal{X} , contains a floating point value indexed on $\langle patient, gene, platform \rangle$ as shown in Figure 1. The size of the first mode spanning over subject or the

Table 1: TCGA PAN Cancer (PanCan12) freeze 4.7 and Synapse repository.

Platform	Input Data	# of Genes	# of Samples
P1. miRNA	syn2491366	14,345	4198
P2. Methylation	syn2486658	1,383	4919
P3. Somatic CNV	syn1710678	876	3260
P4. mRNA	syn1715755	14,178	3599
P5. Somatic SNV	syn1729383	14,351	4933

patient index is 4,555; the size of the second mode spanning over the genes is 14,351; and the size of the third mode spans over five different platforms.

2.1.2 Network constraint formation with pathway data. Links between genes in gene-gene network is used for constraining the factor matrices towards existing knowledge of gene associations. The initial bio-network of human gene associations is retrieved from version 8 of PathwayCommons [2]. The initial bio-network is then used to construct adjacency matrix of gene network for the list of gene considered in the tensor construction. The adjacency matrix, \mathbf{Y} , contains 665,429 number of association information of 14,351 genes.

2.2 Tensor basics

We describe the basic notations and operations on a tensor and its decompositions. Table 2 shows the definitions of symbols used in this paper. A tensor is a generalization of a multi-dimensional array denoted by a boldface Euler script, e.g. \mathcal{X} . An N -mode tensor is denoted as $\mathcal{X} \in \mathbb{R}^{I_1 \times I_2 \times \dots \times I_N}$, and $(i_1 i_2 \dots i_N)$ -th elements of \mathcal{X} is denoted as $x_{i_1 i_2 \dots i_N}$. A matrix is denoted by an uppercase bold letter, e.g. \mathbf{A} . The i -th row vector of \mathbf{A} is denoted by \mathbf{a}_i in lowercase bold letter, and the (ij) -th entry of \mathbf{A} is denoted by a_{ij} . All tensor and matrix indices are positive integers greater than or equal to 1. The mode- n matrix product of a tensor $\mathcal{X} \in \mathbb{R}^{I_1 \times I_2 \times \dots \times I_N}$ with a matrix $\mathbf{A} \in \mathbb{R}^{I_n \times K}$ is denoted by $\mathcal{X} \times_n \mathbf{A}$ and has the size of $I_1 \times \dots \times I_{n-1} \times K \times I_{n+1} \times \dots \times I_N$. The element-wise definition is as follows:

$$(\mathcal{X} \times_n \mathbf{A})_{i_1 \dots i_{n-1} j_{n+1} \dots i_N} = \sum_{i_n=1}^{I_n} x_{i_1 i_2 \dots i_n} a_{j_{n+1} \dots i_N i_n}. \quad (1)$$

See [11] for detailed explanations about tensor operations. We focus on 3-mode tensor $\mathcal{X} \in \mathbb{R}^{I_1 \times I_2 \times I_3}$ for the following sections since our dataset includes a 3-mode tensor (Section 2.1.1).

After construction of tensors, they can be decomposed in several ways. We focus on higher order singular value decomposition (HOSVD).

HOSVD, also known as Tucker decomposition, is the generalization of singular value decomposition (SVD), which works on matrices. HOSVD decomposes a tensor into a core tensor and orthogonal factor matrices corresponding to modes. Specifically, given a 3-mode data tensor \mathcal{X} , HOSVD decomposes \mathcal{X} as follows:

$$\mathcal{X} \approx \tilde{\mathcal{X}} = \mathcal{G} \times_1 \mathbf{U}^{(1)} \times_2 \mathbf{U}^{(2)} \times_3 \mathbf{U}^{(3)}, \quad (2)$$

where $\mathcal{G} \in \mathbb{R}^{J_1 \times J_2 \times J_3}$ is a core tensor, and $\mathbf{U}^{(n)} \in \mathbb{R}^{I_n \times J_n}$ denotes the factor matrices for the n -th dimensions, respectively. HOSVD finds the factors by minimizing the following objective function:

$$\begin{aligned} f &= \frac{1}{2} \|\mathcal{X} - \tilde{\mathcal{X}}\|^2 + \frac{\lambda}{2} R(\mathcal{G}, \mathbf{U}^{(1)}, \mathbf{U}^{(2)}, \mathbf{U}^{(3)}), \\ &= \frac{1}{2} \sum_{(ijk) \in \Omega_{\mathcal{X}}} (x_{ijk} - \mathcal{G} \times_1 \mathbf{u}_i^{(1)} \times_2 \mathbf{u}_j^{(2)} \times_3 \mathbf{u}_k^{(3)})^2 \\ &\quad + \frac{\lambda}{2} R(\mathcal{G}, \mathbf{U}^{(1)}, \mathbf{U}^{(2)}, \mathbf{U}^{(3)}), \end{aligned} \quad (3)$$

where $R(\mathcal{G}, \mathbf{U}^{(1)}, \mathbf{U}^{(2)}, \mathbf{U}^{(3)})$ is the L_2 regularization term. Performance comparison of existing graph constrained HOSVD method is provided in the Supplementary.

Table 2: Table of symbols.

Symbol	Definition
\mathcal{X}	a tensor (boldface Euler script)
x_{ijk}	(ijk) -th entry of \mathcal{X}
\mathbf{A}	a matrix (uppercase, bold letter)
\mathbf{a}_i	the i -th row vector of \mathbf{A} (lowercase, bold letter)
a_{ij}	(ij) -th entry of \mathbf{A}
\times_n	n -mode matrix product
$\ \bullet\ $	Frobenius norm
$*$	Hadamard product
\circ	Outer product
\oslash	Element-wise division
$\Omega_{\mathcal{X}}$	index set of \mathcal{X}
$\Omega_{\mathcal{X}}^{n,i}$	subset of $\Omega_{\mathcal{X}}$ having i as the n -th index
I_n	length of n -th dimension of input tensor \mathcal{X}
J_n	length of n -th dimension of core tensor \mathcal{G}

2.3 SNeCT decomposition

2.3.1 HOSVD optimization with network constraint. Consider that a graph G represents a network between entities of a dimension. For our data tensor with dimensions of (patient, gene, platform), G is the network of genes as explained in Section 2.1.2. G informs the similarities between genes, e.g., gene i and gene j are similar if $y_{ij} = 1$. To include the similarity constraint to HOSVD, the network graph G acts as a regularization as studied in previous works of [13, 18]. Specifically, we add the network regularization term $\lambda_g f_g$ to the objective function of Equation (3) where matrix \mathbf{Y} is the adjacency matrix of G constraining the second dimension, and λ_g is a constant.

$$\begin{aligned} f_g &= \frac{1}{2} \sum_{l=1}^{J_2} \left[\sum_{(k_1 k_2) \in \Omega_Y} y_{k_1 k_2} (u_{k_1 l}^{(2)} - u_{k_2 l}^{(2)})^2 \right] \\ &= \frac{1}{2} \sum_{(k_1 k_2) \in \Omega_Y} y_{k_1 k_2} \|\mathbf{u}_{k_1}^{(2)} - \mathbf{u}_{k_2}^{(2)}\|^2 \end{aligned} \quad (4)$$

where Ω_Y is the index set of \mathbf{Y} . Minimizing f_g guides the algorithm such that the factors of associated genes become similar, i.e., $\mathbf{u}_{j_1}^{(2)}$ and $\mathbf{u}_{j_2}^{(2)}$ have similar values when there is an edge between gene j_1 and gene j_2 in the graph G .

2.3.2 Parallelizable update rules. We present a multi-core algorithm to minimize the objective function $f_{opt} = f + \lambda_g f_g$ and factorize the given tensor \mathcal{X} into HOSVD form. SNeCT adopts parallel stochastic gradient descent (SGD) optimization technique, and thus is highly memory-efficient and scalable to large datasets and multiple cores. We rewrite f so that it forms an SGD-amenable form.

$$f = \frac{1}{2} \sum_{(i_1 i_2 i_3) \in \Omega_{\mathcal{X}}} \left[(x_{i_1 i_2 i_3} - \tilde{x}_{i_1 i_2 i_3})^2 + \frac{\lambda}{|\Omega_{\mathcal{X}}|} \|\mathcal{G}\|^2 + \lambda \sum_{n=1}^3 \frac{\|\mathbf{u}_{i_n}^{(n)}\|^2}{|\Omega_{\mathcal{X}}^{n, i_n}|} \right]$$

Note that f_g already has the SGD-amenable form and $\Omega_{\mathcal{X}}$ excludes the cells with missing data. Now, gradients of f_{opt} with respect to factors for a given data point $x_{\alpha=(i_1 i_2 i_3)}$ or $y_{\beta=(k_1 k_2)}$ are calculated as follows:

Algorithm 1 SNeCT

Input: Input data: tensor $\mathcal{X} \in \mathbb{R}^{I_1 \times I_2 \times \dots \times I_N}$, network matrix $\mathbf{Y} \in \mathbb{R}^{I_c \times K}$, number of parallel cores P , and network-constrained mode c
 Hyperparameters: core size (J_1, J_2, \dots, J_N) , learning rate η , and regularization factors λ and λ_g
Output: Core tensor $\mathcal{G} \in \mathbb{R}^{J_1 \times J_2 \times \dots \times J_N}$, and factor matrices $\mathbf{U}^{(1)}, \mathbf{U}^{(2)}, \dots, \mathbf{U}^{(N)}$

- 1: Initialize $\mathcal{G}, \mathbf{U}^{(n)} \in \mathbb{R}^{I_n \times J_n}$ for $n = 1, 2, \dots, N$ randomly
- 2: **repeat**
- 3: **for** $\forall x_{i_1 i_2 \dots i_N} \in \mathcal{X}, \forall y_{k_1 k_2} \in \mathbf{Y}$ in random order **do in parallel**
- 4: **if** $x_{i_1 i_2 \dots i_N} \in \mathcal{X}$ is picked **then**
- 5: Cache intermediate data tensor: $\mathcal{D} \leftarrow \mathcal{G} * (\mathbf{u}_{i_1}^{(1)} \circ \mathbf{u}_{i_2}^{(2)} \circ \dots \circ \mathbf{u}_{i_N}^{(N)})$
- 6: $\tilde{x}_{i_1 i_2 \dots i_N} \leftarrow$ sum of all elements of \mathcal{D}
- 7: Update corresponding factor rows: $\mathbf{u}_{i_n}^{(n)} \leftarrow \mathbf{u}_{i_n}^{(n)} - \eta((\tilde{x}_{i_1 i_2 \dots i_N} - x_{i_1 i_2 \dots i_N}) \cdot \text{Collapse}(\mathcal{D}, n) + \frac{\lambda}{|\Omega_{\mathcal{X}}^{n, i_n}|} \mathbf{u}_{i_n}^{(n)})$, (for $n = 1, 2, \dots, N$)
- 8: Update core tensor: $\mathcal{G} \leftarrow \mathcal{G} - \eta P((\tilde{x}_{i_1 i_2 \dots i_N} - x_{i_1 i_2 \dots i_N}) \cdot \mathcal{D} \oslash \mathcal{G} + \frac{\lambda}{|\Omega_{\mathcal{X}}|} \mathcal{G})$, (executed by only one core)
- 9: **end if**
- 10: **if** $y_{k_1 k_2} \in \mathbf{Y}$ is picked **then**
- 11: Update network-constrained factors: $\mathbf{u}_{k_1}^{(c)} \leftarrow \mathbf{u}_{k_1}^{(c)} - \eta \lambda_g y_{k_1 k_2} (\mathbf{u}_{k_1}^{(c)} - \mathbf{u}_{k_2}^{(c)})$, $\mathbf{u}_{k_2}^{(c)} \leftarrow \mathbf{u}_{k_2}^{(c)} - \eta \lambda_g y_{k_1 k_2} (\mathbf{u}_{k_2}^{(c)} - \mathbf{u}_{k_1}^{(c)})$
- 12: **end if**
- 13: **end for**
- 14: **until** convergence conditions are satisfied
- 15: $\mathbf{Q}^{(n)}, \mathbf{R}^{(n)} \leftarrow$ QR decomposition of $\mathbf{U}^{(n)}, \mathbf{U}^{(n)} \leftarrow \mathbf{Q}^{(n)}, \mathcal{G} \leftarrow \mathcal{G} \times_n \mathbf{R}^{(n)}$, (for $n = 1, 2, \dots, N$)
- 16: **return** $\mathcal{G}, \mathbf{U}^{(1)}, \mathbf{U}^{(2)}, \dots, \mathbf{U}^{(N)}$

$$\begin{aligned} \left. \frac{\partial f_{opt}}{\partial \mathbf{u}_{i_1}^{(1)}} \right|_{\alpha} &= -(x_{\alpha} - \tilde{x}_{\alpha}) [\mathcal{G} \times_2 \mathbf{u}_{i_2}^{(2)} \times_3 \mathbf{u}_{i_3}^{(3)}] + \frac{\lambda}{|\Omega_{\mathcal{X}}^{1, i_1}|} \mathbf{u}_{i_1}^{(1)} \\ \left. \frac{\partial f_{opt}}{\partial \mathcal{G}} \right|_{\alpha} &= -(x_{\alpha} - \tilde{x}_{\alpha}) \times_1 \mathbf{u}_{i_1}^{(1)\top} \times_2 \mathbf{u}_{i_2}^{(2)\top} \times_3 \mathbf{u}_{i_3}^{(3)\top} + \frac{\lambda}{|\Omega_{\mathcal{X}}|} \mathcal{G} \quad (5) \\ \left. \frac{\partial f_{opt}}{\partial \mathbf{u}_{k_1}^{(2)}} \right|_{\beta} &= \lambda_g y_{\beta} (\mathbf{u}_{k_1}^{(2)} - \mathbf{u}_{k_2}^{(2)}) \end{aligned}$$

$\left. \frac{\partial f_{opt}}{\partial \mathbf{u}_{i_2}^{(2)}} \right|_{\alpha}$, $\left. \frac{\partial f_{opt}}{\partial \mathbf{u}_{i_3}^{(3)}} \right|_{\alpha}$, and $\left. \frac{\partial f_{opt}}{\partial \mathbf{u}_{k_2}^{(2)}} \right|_{\beta}$ are calculated symmetrically as the above equations. The above equations are naturally generalized to mode- N tensors.

3.3.3 SNeCT learning model. SNeCT optimizes the objective function f_{opt} by parallel SGD update. Algorithm 1 shows detailed procedures of decomposition of a general N -mode tensor \mathcal{X} and network constraint \mathbf{Y} which represents the similarity of c -th mode entities.

In the beginning, SNeCT initializes $\mathbf{U}^{(1)}, \mathbf{U}^{(2)}, \dots, \mathbf{U}^{(N)}$, and \mathcal{G} randomly (line 1 of Algorithm 1). The outer loop (lines 2-14) repeats until the factors converge. In the inner loop (lines 3-13), SNeCT conducts parallel updates of factor rows corresponding to each data point $x_{i_1 i_2 i_3}$ or $y_{j_1 j_2}$ in random order. When calculating gradients with respect to factor rows and core tensor, it takes excessive time to calculate $\tilde{x}_{alpha} = \mathcal{G} \times_1 \mathbf{u}_{i_1}^{(1)} \times_2 \dots \times_n \mathbf{u}_{i_N}^{(N)}$ and tensor-matrix products for $\left. \frac{\partial f_{opt}}{\partial \mathbf{u}_{i_n}^{(n)}} \right|_{\alpha}$ every time when they are needed. SNeCT reduces the time cost efficiently by caching intermediate data tensor \mathcal{D} (line 5). See section 3.5 of [4] for detailed approach of utilizing intermediate data to reduce time cost. *Collapse*(\mathcal{D}, n) operator (line

7) outputs a vector with length of i_n which contains the sum of k -th slice of D over n -th mode as its k -th element. In line 8, element-wise division operator \oslash is used to efficiently calculate core tensor gradient.

There are possible conflicts between the parallel updates since a factor row or core tensor might be accessed by multiple update attempts. However, we apply lock-free parallel update scheme [4, 21] and remove frequent conflicts by updating core tensor using only one core (line 6); thus SNeCT guarantees near-linear convergence to a local optimum.

3 RESULTS

3.1 Stratification

3.1.1 Cluster assignment. We perform cluster analysis with k -means clustering algorithm on patient profiles using Euclidean distance. (Euclidean, cosine and Mahalanobis distance measures have been tested with no significant differences in the results.) To generate patient profiles, SNeCT decompose the data tensor as shown in Fig. 1 with core size $[J_1, J_2, J_3] = [78, 48, 5]$, where the best core size was searched with a small validation tensor and graph constraint is set to $\lambda = 1.0$. After decomposition, the rows of patient factor matrix $U^{(1)}$ is used as patient profiles. To find the cluster size we compute the gap statistics introduced by [28]. The gap statistics of the cluster stabilizes after cluster size of 10 as shown in Supplementary Fig. 3. For convenience of comparison, we stratified patient profiles into 13 clusters as suggested in [5]. Table 3 shows the number of assigned patients of twelve cancer types for each cluster.

3.1.2 Survival analysis. We performed survival analysis for the thirteen clusters acquired from Section 3.1.1, using the Cox proportional hazards regression model in the R survival package (Fig 2). We use right-censored survival data for patients: days to death for

Table 3: 12 pathological disease types assigned to clusters of profiles factorized from tensor factorization with graph constraint of $\lambda = 1.0$.

	C1	C2	C3	C4	C5	C6	C7	C8	C9	C10	C11	C12	C13	Total
BLCA	16	32	2	19	0	22	3	0	0	0	32	0	0	126
BRCA	17	3	600	172	1	70	0	0	0	0	26	0	0	889
COAD	4	0	2	2	0	91	317	0	0	0	1	2	0	419
GBM	4	1	1	2	3	7	0	0	248	0	1	0	0	267
HNSC	0	242	1	6	0	1	0	0	0	0	60	0	0	310
KIRC	14	1	1	0	471	4	0	0	1	0	6	0	0	498
LAML	0	0	0	0	0	9	0	0	0	188	0	0	0	197
LUAD	302	2	2	7	1	12	0	0	0	0	29	0	0	357
LUSC	26	32	0	29	0	7	0	0	0	0	246	0	0	340
OV	0	0	1	3	0	1	1	348	0	0	0	0	131	485
READ	1	1	0	5	0	9	145	0	0	0	1	1	0	163
UCEC	3	1	3	117	1	348	1	0	0	0	10	13	2	499
Total	387	315	613	362	477	581	467	348	249	188	412	17	134	4550

dead patients, and days to last contact for alive patients as right-censored data. To see how the network constraint affects decomposition result, we impose three different levels of network regularization: λ_g value of 0 (not constrained), 0.1, and 1. The log-rank statistics value for $\lambda_g = 0$ is 409, for $\lambda_g = 0.1$ is 1151, and for $\lambda_g = 1$ is 1185. The Figure 2 and the log-rank statistics values show that having graph constraint is better, however, little difference is observed for the two weight values.

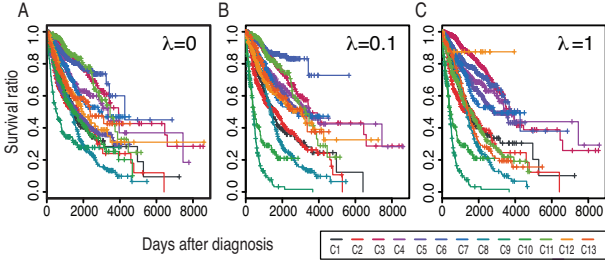


Figure 2: Predicted survival curves for clustered patients. x-axis is survival time (day) and y-axis is survival rate.

3.1.3 Unique cohort clusters. Cluster result of the patient factor matrix, $U^{(1)}$, correlates with tissue of origin which is similar to observation made by [5]. Six clusters, C1-LUAD-enriched, C3-BRCA/Luminal, C5-KIRC, C8-OV-1, C9-GBM, C10-LAML, and C13-OV-2 each dominantly contains cancer samples from a single tissue of origin. Patients in C1-LUAD-enriched cluster includes 302 out of 357 LUAD patients with relatively good prognosis, that is, neoplasm cancer status is tumor free for 186 out of all 217 tumor free cases with precision of 0.73 (recall of 0.85). Patients in C3-BRCA/Luminal cluster groups 600 BRCA cases with 13 other cancer types. The BRCA patients in C3 have positive estrogen and progesterone receptor status with precision of 0.95 and 0.85, respectively, and HER2 status is mixed tending to have more negative status with precision of 0.73. Furthermore, C3 contains 8 out of 9 metastatic cases and contains 34 out of 43 cases with known other malignancy histological type. It tells us that C3 groups patients with BRCA Luminal A and Luminal B molecular subtypes of breast cancer. Four other clusters that form somewhat mutually exclusive collectively exhaustive groups are cluster C5-KIRC that contains 471 patients classified as KIRC and 6 patients classified

to other cancer types, cluster C9-GBM that contains 248 cases of GBM patients with only one of KIRC patient, cluster C10-LAML that contains 188 cases of LAML with no other cancer patients included, and cluster C12-UCEC-small, a small cluster, that contains 13 UCEC with 4 other cases with very high survival ratio as shown in Fig. 3(c).

Interestingly, two clusters are formed for OV cases: C13-OV-2 that contains 131 cases of OV patient with only three other cancer types and cluster C8-OV-1 that contains 348 cases of OV patients with no other cancer type. There is no clear distinction between the clinical features of the two clusters. However, a clear distinction can be found comparing factor values of genomic contents for C13, C8, and other clusters, as shown in Supplementary Fig. 4(a). Separation can also be found in the survival analysis of C8 and C13 (Fig. 3(a)). Another interesting cluster is C7-COAD/READ that combines two colorectal tumor samples from cohorts COAD and READ with C7 READ containing almost all READ cases (145 out of 163). C7 COAD group contains 22 (precision 1 and recall of 0.88) normal braf gene analysis results while C6 COAD contains all three cases of abnormal braf gene analysis result. C7 COAD tends to have better survival ratio compared to C6 COAD cases as shown in Supplementary Fig. 5.

3.1.4 Squamous-like cluster. Patients in the C2-HNSC-enriched-squamous-like cluster contains squamous-like BLCA (32), HNSC (242), and LUSC (32) of mostly male (228/315) patients. 242 out of 310 HNSC patients are group to C2 where 60 other HNSC patients are grouped in another squamous-like cluster C11 that contains 246 out of 340 LUSC patients. Also, within C2 cluster, BLCA group contains 26 patients diagnosed as non-papillary with a precision of 0.79 and mixed neoplasm cancer status (14 tumor free and 13 with tumor) and contains 9 cases of having other malignancy histological type. LUSC and HNSC patients in group C2 do not show clear characteristics in terms of clinical features other than being skewed towards male gender. Cluster C11-LUSC-enriched-squamous-like contains a mixed group of 32 BLCA, 26 BRCA, 60 HNSC, 29 LUAD, and 246 LUSC cancer patients. The LUSC cases within C11 contains 128 patients and tends to be skewed towards patients with higher level of smoking history (level 4 - 130/174, level 3 - 43/67, level 2 61/79 and level 1 - 6/13) but with slightly better prognosis (tumor free 142 out of 198 and with tumor 38 out of 56); HNSC patients in C11 have mixed neoplasm cancer statuses (tumor free 36 and with tumor 18) and are mostly of intermediate histological grade (41 of grade g2 and 15 of grade g3). BRCA patients in the group tend to have negative progesterone receptor status (20 negatives; 4 positives), negative estrogen receptor status (16 negatives; 8 positives), negative HER2 status (14 negatives; 3 positives; 3 equivocal), contains many (24) infiltrating ductal carcinoma cases, and tend to have the worst prognostics (Fig. 3(a)).

3.1.5 BRCA/UCEC clusters. Two BRCA/UCEC-enriched clusters are formed as C4 and C6. C4-BRCA/UCEC-enriched cluster contains 172 BRCA and 117 UCEC cases mixed with 29 LUSC and 19 BLCA cases. C6-BRCA/UCEC-enriched cluster contains 70 BRCA and 348 UCEC cases mixed with 90 COAD and 22 BLCA cases. Patients in C4 BRCA has mostly negative estrogen receptor status

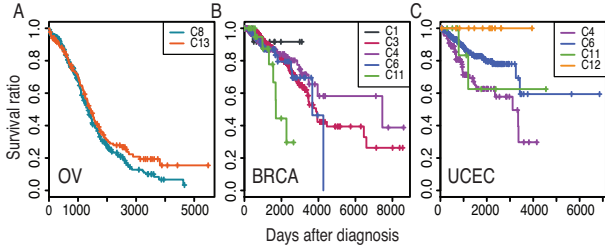


Figure 3: Survival analysis of clusters for cohorts OV (A), BRCA (B), and UCEC (C).

(127 negative cases with precision 0.77; 38 positives), mostly negative progesterone receptor status (131 negatives; 32 positives; 1 intermediate), and mostly negative her2 status (101 negatives; 23 positives; 23 equivocal). The group also contains all 5 of medullary carcinoma cases. 70 BRCA patients in C6, on the other hand, have mixed positive and negative status for both progesterone receptor estrogen receptor and mostly negative HER2 status (38 negatives; 8 positives; 9 others). Also, survival analysis shows higher ratio of patients surviving longer for C4-BRCA compared to C6-BRCA. The clinical characteristics and the survival analysis show that C4 UCEC groups patients with poor prognostic. That is, C4 UCEC includes higher ratio of serous adenocarcinoma (69/115) cases than the common endometrioid carcinoma (45/378); the tumor grades of the group tend to be high with 7 high-grades (out of 11 possible) and 100 grade-3; 12 out of 30 cases are with known as ‘other malignancy histological type’ within the group; and the group shows the fastest drop of survival rates in the Kaplan-Meier plot (Fig. 3(b).) On the other hand, UCEC patients grouped in C6 show better prognostic. That is, the C6 UCEC includes large portion of endometrioid carcinoma (312/375, precision of 0.89), large portion of tumor free neoplasm cancer status (292/393, precision of 0.88), large portion of low to intermediate histological grades (g1 - 87/91, g2 - 93/106), and approximately half of grade 3 and little of grade 4 (3 out of 11). Also, their survival ratio drop rate is less dramatic compared to C4 UCEC cases.

3.2 Prediction

3.2.1 Top-k search. When a new query patient q arrives with data \mathcal{X}_q which is a tensor representing the patient profile of q , we aim to find the SNeCT factor for the patient using the pre-calculated factor matrices and core tensor. Thus we compare the factors of other patients which are encoded in the patient factor matrix $\mathbf{U}^{(1)}$ with the calculated patient factor. We solve the following equation with the SNeCT algorithm while fixing parameters other than \mathbf{u} .

$$\mathbf{u}_q = \arg \min_{\mathbf{u}} \|\mathcal{X}_q - \mathcal{G} \times_1 \mathbf{u} \times_2 \mathbf{U}^{(2)} \times_3 \mathbf{U}^{(3)}\|. \quad (6)$$

After generation of new profile, \mathbf{u}_q , it is used to seek top- k similar patients by calculating the distance between the query factor and patient factors. It takes 550ms on average to search for a query against the training set.

3.2.2 Clinical similarity of top-k search. To test the clinical prediction accuracy of SNeCT, we generated the factor matrices from 90% of the data and used 10% of the data as test set or new queries and determined the clinical similarity of the query patient to the

Table 4: Top-k search precision.

Cohort	Clinical Features	Top 1	Top 5	Top 10	Top R
BRCA	estrogen receptor status	0.72	0.85	0.86	0.81
	progesterone receptor status	0.86	0.71	0.71	0.68
	her2/neu IHC receptor status	0.53	0.51	0.49	0.55
	neoplasm cancer status	0.84	0.80	0.81	0.77
COAD	braf gene analysis result	1.00	0.80	0.70	0.92
	colon polyps present	0.47	0.56	0.52	0.59
	1st relatives with cancer	0.84	0.78	0.75	0.84
	venous invasion	0.61	0.60	0.63	0.72
GBM	histological type	0.96	0.94	0.94	0.78
	icd-o-3 histology	1.00	1.00	1.00	0.77
	neoplasm cancer status	0.85	0.82	0.83	0.77
HNSC	hpv status by p16 testing	0.78	0.78	0.77	0.73
	histological type	1.00	0.99	0.99	0.73
KIRC	icd-o-3 histology	1.00	0.99	0.99	0.73
	number packs/year smoked	0.50	0.30	0.20	1.00
	calgb cytogenetics risk cat.	0.85	0.84	0.81	0.65
LAML	neoplasm histologic grade	0.79	0.75	0.76	0.77
READ	braf gene analysis result	1.00	1.00	1.00	1.00
	1st relatives with cancer	0.93	0.77	0.78	0.86
UCEC	menopause status	0.71	0.76	0.76	0.77
	neoplasm cancer status	0.83	0.75	0.77	0.77

top- k similar patients searched against factor matrix $\mathbf{U}^{(1)}$. Then we evaluated the average precision over test cases for each selected clinical features on top-1, top-5, top-10, and top- R search results, where the R value computes the number of samples with the same clinical values as the query in the database and varies from query to query. Overall, ‘‘age at initial pathologic diagnosis’’ and ‘‘vital status’’ coincide well with all top- k retrievals with average precision over all the test data ranging from 0.76 to 0.81 and from 0.66 to 0.68, respectively. No significant features were found for LUAD, LUSC, and BLCA other than the two clinical features. Other clinical features that are cohort-specific or have high average precision values are listed in Table 4. Looking at the precision values, we can see that the search successfully retrieved BRCA patients with similar estrogen and progesterone receptor status in most cases while less so in terms of her2/neu IHC receptor status. Also, most search results matched that of the query for the braf gene analysis results in the COAD and READ test cases.

3.3 Personalized subtype analysis scenario

The most valuable aspects of tensor factorization results are on the possibility of personalized interpretation of given patients. To illustrate how factor matrices can be used for personalized interpretation, we provide a brief example on a given patient i . For the patient i , SNeCT generates patient profile $\mathbf{u}_i^{(1)}$. If the patient is a new patient we can use the Eq. 6 to generate the profile. We then calculate the personalized subtype matrix as follows: $\mathcal{S} = \mathcal{G} \times_1 \mathbf{u}_i^{(1)}$ ($\in \mathbb{R}^{J_2 \times J_3}$). \mathcal{S} provides a personalized weight information for subtypes for the gene and the platform modes. For the sample TCGA-BS-A0UV, the center of Fig. 4 shows the heatmap of \mathcal{S} . Each row of \mathcal{S} represents a subtype for gene mode, thus norm of each row represents the influence of each subtype to the patient. Each column of $\mathcal{S} \times_3 \mathbf{U}^{(3)}$ represents the platform mode. The norm of each column shows the influence of each platform to the patient and right side of Fig. 4 shows the associated factor values. With the analysis,

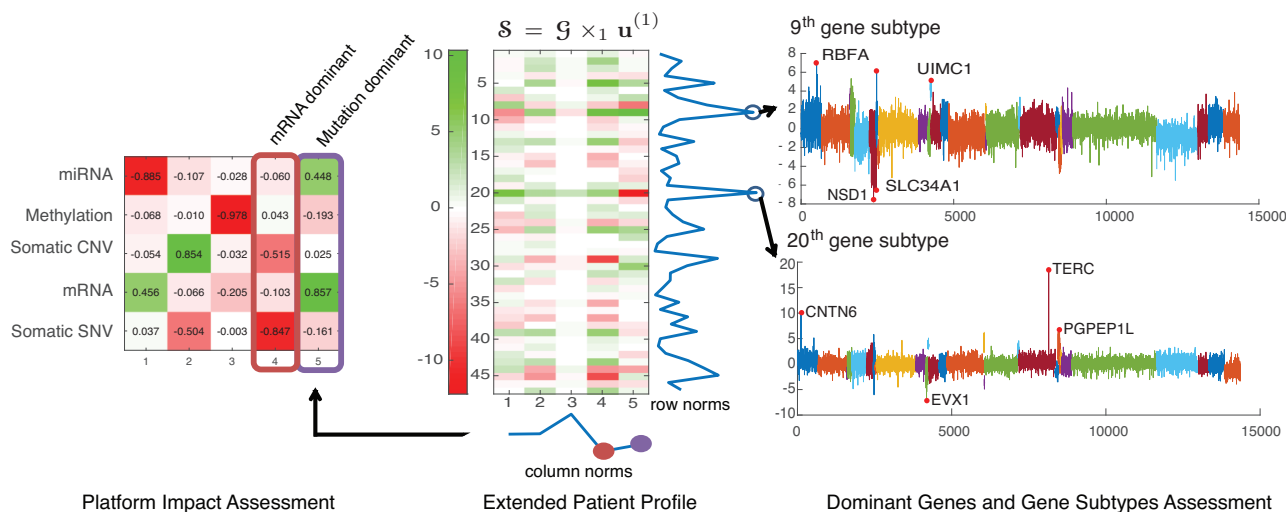


Figure 4: Personalized analysis example of patient ID TCGA-BS-A0UV in cohort UCEC assigned to cluster C12.

we can determine which gene subtypes dominantly characterize the patient and which platform data were important in finding the dominant characteristics such that we can trace back to the significant genes and the type of abnormality.

4 DISCUSSION AND CONCLUSIONS

In this paper, we have proposed a large-scale network constrained Tucker decomposition method (SNeCT) that is based on parallelizable stochastic gradient descent. With SNeCT, it is possible to systematically analyze high dimensional multi-platform genomic data constrained on prior knowledge of feature associations in a form of a network. It is a general purpose approach that can be applied in various combinations of multi-platform data. This is important as the availability and variety of multi-platform genomic data increases and the need for fast and intuitive methods becomes higher. However, existing methods either run in a small-scale analysis, combine multiple analysis methods thus requiring a large number of hyper-parameter tuning and expert knowledge. The practicality of SNeCT was shown on the PANCAN12 dataset where the stratification result shows a high correlation to subsets of clinical features and to the tissue of origin, which is consistent with the observation made by [5]. Also, SNeCT can be applied to search for top- K similar patients given a new patient, which has various utilities such as using the clinical features of top- k patients in diagnostics and prognostic predictions. Furthermore, we showed how the combination of factor matrices can be used for personalized genomic interpretation of a patient. There are considerations to make when using SNeCT, such as choosing normalization and gene mapping methods for construction of the input tensor, sizes of latent factors, appropriate network, number of clusters in stratification studies, and value of K in the top- K search in the clinical predictions. However, these are common problems in analysis and several solutions can be found in existing literature. We conclude that SNeCT provides a powerful tool for integrative analysis of multi-platform to the bioinformatics community.

FUNDING

This research was supported by Basic Science Research Program through the NRF of Korea (NRF-2015R1C1A2A01055739) and by the KEIT Korea under the “Global Advanced Technology Center” (10053204).

REFERENCES

- [1] Carlson, A., Betteridge, J., Kisiel, B., Settles, B., Jr., E.R.H. and Mitchell, T.M. (2010) Toward an architecture for never-ending language learning. In *Proceedings of AAAI 2010, Atlanta, Georgia, USA*.
- [2] Cerami, E.G., Gross, B.E., Demir, E., Rodchenkov, I., Babur, Ö., Anwar, N., Schultz, N., Bader, G.D. and Sander, C. (2011) Pathway Commons, a web resource for biological pathway data. *Nucleic Acids Research*, **39** (SUPPL. 1).
- [3] Chang, K., Yih, W. and Meek, C. (2013) Multi-relational latent semantic analysis. In *Proceedings of EMNLP 2013, Seattle, Washington, USA* pp. 1602–1612.
- [4] Choi, D., Jang, J.G. and Kang, U. (2017) Fast, accurate, and scalable method for sparse coupled matrix-tensor factorization. *arXiv preprint arXiv:1708.08640*.
- [5] Hoadley, K.A., Yau, C., Wolf, D.M., Cherniack, A.D., Tamborero, D., Ng, S., Leiser, M.D.M., Niu, B., McLellan, M.D., Uzunangelov, V., et al. (2014) Multiplatform analysis of 12 cancer types reveals molecular classification within and across tissues of origin. *Cell*, **158** (4), 929–944.
- [6] Jeon, B., Jeon, I., Sael, L. and Kang, U. (2016a) SCouT: Scalable coupled matrix-tensor factorization - algorithm and discoveries. In *Proceedings of IEEE ICDE 2016, Helsinki, Finland*.
- [7] Jeon, I., Papalexakis, E.E., Faloutsos, C., Sael, L. and Kang, U. (2016b) Mining billion-scale tensors: algorithms and discoveries. *VLDB J.*, **25** (4), 519–544.
- [8] Kim, S., Sael, L. and Yu, H. (2014) Identifying cancer subtypes based on somatic mutation profile. In *Proceedings of the DTMBIO '14* New York, NY, USA.
- [9] Kim, S., Sael, L. and Yu, H. (2015) A mutation profile for top- k patient search exploiting Gene-Ontology and orthogonal non-negative matrix factorization. *Bioinformatics*, **31** (22), 3653–3659.
- [10] Kolda, T. and Bader, B. (2006) The TOPHITS model for higher-order web link analysis. In *Workshop on Link Analysis, Counterterrorism and Security*, **7**, 26–29.
- [11] Kolda, T.G. and Bader, B.W. (2009) Tensor decompositions and applications. *SIAM review*, **51** (3), 455–500.
- [12] Kolda, T.G. and Sun, J. (2008) Scalable tensor decompositions for multi-aspect data mining. In *Proceedings of ICDM 2008* pp. 363–372.
- [13] Li, W.J. and Yeung, D.Y. (2009) Relation regularized matrix factorization. In *Proceedings of IJCAI 2009* p. 1126.
- [14] Louhimo, R. and Hautaniemi, S. (2011) CNAmets: an R package for integrating copy number, methylation and expression data. *Bioinformatics*, **27**, 887–888.
- [15] Mankoo, P.K., Shen, R., Schultz, N., Levine, D.A. and Sander, C. (2011) Time to recurrence and survival in serous ovarian tumors predicted from integrated genomic profiles. *PLoS One*, **6** (11), e24709.
- [16] Maruhashi, K., Guo, F. and Faloutsos, C. (2011) MultiAspectForensics: Pattern mining on large-scale heterogeneous networks with tensor analysis. In *Proceedings of ASONAM 2011* pp. 203–210.

- [17] Mo,Q., Wang,S., Seshan,V.E., Olshen,A.B., Schultz,N., Sander,C., Powers,R.S., Ladanyi,M. and Shen,R. (2013) Pattern discovery and cancer gene identification in integrated cancer genomic data. *Proceedings of the National Academy of Sciences*, **110** (11), 4245–4250.
- [18] Narita,A., Hayashi,K., Tomioka,R. and Kashima,H. (2012) Tensor factorization using auxiliary information. *Data Mining and Knowledge Discovery*, **25** (2), 298–324.
- [19] Nickel,M., Tresp,V. and Kriegel,H. (2012) Factorizing YAGO: scalable machine learning for linked data. In *Proceedings of WWW 2012, Lyon, France*. pp. 271–280.
- [20] Omberg,L., Ellrott,K., Yuan,Y., Kandoth,C., Wong,C., Kellen,M.R., Friend,S.H., Stuart,J., Liang,H. and Margolin,A.a. (2013) Enabling transparent and collaborative computational analysis of 12 tumor types within The Cancer Genome Atlas. *Nature Genetics*, **45** (10), 1121–1126.
- [21] Recht,B., Re,C., Wright,S. and Niu,F. (2011) Hogwild: a lock-free approach to parallelizing stochastic gradient descent. In *Advances in Neural Information Processing Systems* pp. 693–701.
- [22] Sael,L., Jeon,I. and Kang,U. (2015) Scalable tensor mining. *Big Data Research*, **2** (2), 82–86.
- [23] Shin,K., Sael,L. and Kang,U. (2017) Fully scalable methods for distributed tensor factorization. *IEEE TKDE*, **29** (1), 100–113.
- [24] Sohn,K.A., Kim,D., Lim,J. and Kim,J.H. (2013) Relative impact of multi-layered genomic data on gene expression phenotypes in serous ovarian tumors. *BMC Systems Biology*, **7**, S9.
- [25] Sun,J., Papadimitriou,S. and Yu,P.S. (2006) Window-based tensor analysis on high-dimensional and multi-aspect streams. In *Proceedings of ICDM 2006*, pp. 1076–1080.
- [26] Thomas,J. and Sael,L. (2015) Overview of integrative analysis methods for heterogeneous data. In *Proceedings of BigComp 2015*, pp. 266–270.
- [27] Thomas,J. and Sael,L. (2016) Maximizing information through multiple kernel-based heterogeneous data integration and applications to ovarian cancer. In *Proceedings of EDB 2016* pp. 97–100 ACM Press.
- [28] Tibshirani,R., Walther,G. and Hastie,T. (2001). Estimating the number of clusters in a data set via the gap statistic. *Series B Statistical Methodology* **63** (2), 411–423.
- [29] Vaske,C.J., Benz,S.C., Sanborn,J.Z., Earl,D., Szeto,C., Zhu,J., Haussler,D. and Stuart,J.M. (2010) Inference of patient-specific pathway activities from multi-dimensional cancer genomics data using PARADIGM. *Bioinformatics*, **26** (12), i237–45.
- [30] Yuan,Y., Van Allen,E.M., Omberg,L., Wagle,N., Amin-Mansour,A., Sokolov,A., Byers,L.a., Xu,Y., Hess,K.R., Diao,L., et al. (2014) Assessing the clinical utility of cancer genomic and proteomic data across tumor types. *Nature Biotechnology*, **32** (7), 644–652.